Materials Advances

ROYAL SOCIETY OF CHEMISTRY

PAPER

View Article Online
View Journal | View Issue

Cite this: *Mater. Adv.*, 2025, **6**, 4132

Exploring the dynamic behaviour and optical properties of indolocarbazole charge-transfer cocrystals†

Jade Cisneros, [a] Ernesto A. Hernández-Morales, [a] Armando Navarro-Huerta, [a] Jan Blahut, [b] Erika Bartůňková,[b] Simon J. Teat, [c] Rubén A. Toscano,[a] Martin Dračínský *[b] and Braulio Rodríguez-Molina *[a]

Received 2nd May 2025,
Accepted 15th May 2025

DOI: 10.1039/d5ma00425j

rsc.li/materials-advances

Organic charge-transfer cocrystals offer a well-established route to engineer crystalline materials by strategically selecting their coformers. Herein, we report two novel cocrystals with indolo[3,2,1-*jk*]-carbazole as a donor molecule with two different components: 7,7,8,8-tetracyanoquinodimethane (**ICZ-TCNQ**) and tetrafluoro-1,4-benzoquinone (**ICZ-TFBQ**). The degree of charge transfer (DCT) was elucidated in both cocrystals through the use of FTIR and diffuse reflectance spectroscopic studies. The **ICZ-TCNQ** cocrystal shows photothermal conversion properties with an efficiency of 12.8 ± 2.1% at 0.52 W cm^{-2}. Moreover, the **ICZ-TFBQ** cocrystal shows thermally-driven rotational motions of the **TFBQ** fragment, reaching hundreds of MHz at *ca.* 348 K, as evidenced by ^{19}F T_1 relaxation measurements and ^{13}C CPMAS solid-state NMR experiments. Contrasting **ICZ-TCNQ** and **ICZ-TFBQ** cocrystals, our study offers a broad perspective on the structural and functional versatility of **ICZ**-based systems, providing deeper comprehension into their optical and dynamic behaviour.

Introduction

The field of organic electronics has experienced significant growth due to the chemical versatility and low cost of organic materials. Researchers have focused on designing and developing new strategies to create devices with tunable optical and electronic properties for next-generation optoelectronic applications.[1] Among other efforts, charge-transfer (CT) cocrystals have been established as promising materials, thanks to efficient and direct preparation methods, with excellent performance in properties such as conductivity,[2] charge transport,[3] ferroelectricity,[4] dielectric behaviour,[5] and optical waveguiding.[6] The dense arrangement within these materials often causes molecular crystals to be regarded as 'frozen' molecules capable of only restricted vibrations.

Molecular motions in solids have been extensively studied in several fields of chemistry to design novel materials.[7–9] Prominent examples are artificial molecular machines, which focus on the development of systems that mimic the functionality of biological machines, such as proteins, or emulate the correlated motion of macroscopic industrial gears through the control of molecular dynamics.[10–15] In particular, molecular rotors represent a promising strategy for transducing molecular-level functions to the macroscopic scale. These highly ordered structures, composed of static groups (stator) with dynamic components (rotator), are assembled around a rotational axis (Fig. 1a), which is not limited to covalent bonds but can also be formed by hydrogen bonds, halogen bonds, or π-stacking.[15] Within rigid crystalline lattices, these molecular rotors achieve their dynamic behaviour through a delicate balance of molecular symmetry, structural factors such as cavity shape (free volume), and the resulting intermolecular interactions. These elements modulate the rotational barriers, thereby either enabling or restricting the rotor's motion.[16–18]

An excellent platform for producing internal-motion crystals involves developing CT cocrystals. These multicomponent crystalline solids, composed of the electron-rich donor (D) and electron-poor acceptor (A) molecules (Fig. 1b), interact *via* π-stacking, leading to orbital overlap between their constituent

[a] *Instituto de Química, Universidad Nacional Autónoma de México, Circuito Exterior S/N, Ciudad Universitaria, Coyoacán 04510, Mexico City, Mexico. E-mail: brodriguez@iquimica.unam.mx*
[b] *Institute of Organic Chemistry and Biochemistry, Czech Academy of Sciences, 160 00 Prague, Czech Republic. E-mail: martin.dracinsky@uochb.cas.cz*
[c] *Advanced Light Source, Lawrence Berkeley National Laboratory, Berkeley, California 94720-8229, USA*

† Electronic supplementary information (ESI) available: Synthetic and experimental procedures, spectroscopic data (NMR, FTIR, HRMS), final crystallographic refinement parameters, PXRD diffractograms, Hirshfeld surface maps, DFT computational details, thermal analyses, and PTC measurements. CCDC 2421738–2421740, 2421742, 2421752, 2421754 and 2421755. For ESI and crystallographic data in CIF or other electronic format see DOI: **https://doi.org/10.1039/d5ma00425j**

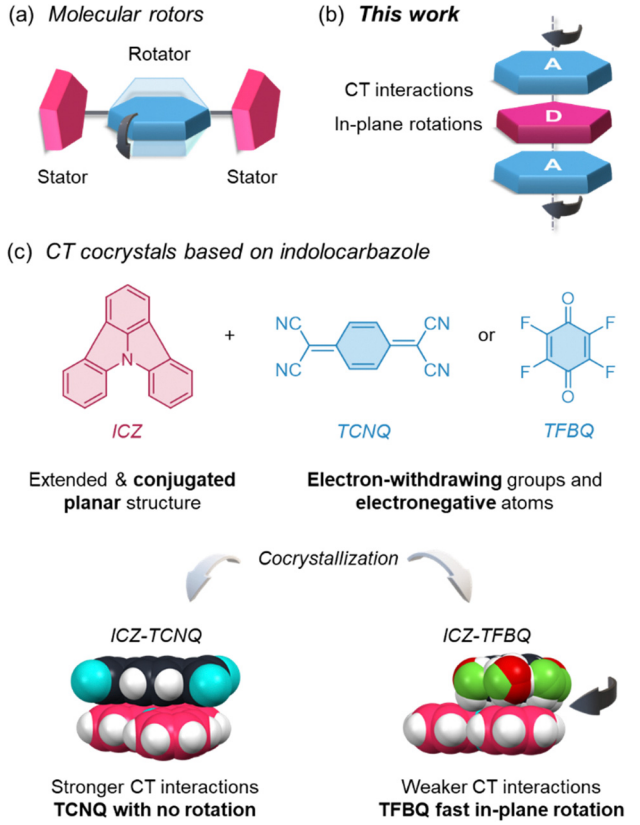

Fig. 1 Schematic illustration of motion (a) in a molecular rotor and (b) in this work. (c) The design of the new CT cocrystals is reported here, with the molecular motion in one instance.

moieties. This interaction induces an intermolecular CT phenomenon, modifying the relative energies of the Frontier molecular orbitals (FMOs) and resulting in a narrowed optical gap (E_g), allowing the fine-tuning of their electronic and optical properties.[19] The ability to tune FMOs through CT interactions has also paved the way for the development of new organic materials, including those with semiconducting[20] and optical waveguiding properties.[21–23]

For instance, the motion of the cyano groups in cocrystals containing tetracyanoquinodimethane (**TCNQ**) and the molecular motions of pyrene in ternary cocrystals have been shown to increase non-radiative energy decay, improving the photothermal conversion efficiency.[24,25] In the realm of dielectric properties, the formation of CT cocrystals has enhanced the in-plane reorientations of molecules such as tetrabromophthalic anhydride and tetraclorophthalonitrile, resulting in high dielectric constants due to dynamics between multiple orientations.[26,27]

The dynamic behavior observed in CT cocrystals is closely linked to both the strength of donor/acceptor interactions and the structural features of the coformers. In systems with weak CT interactions, the resulting crystal lattice tends to be less rigid, allowing for greater rotational freedom of the constituent molecules and in some cases, the presence of large donor molecules or pseudo-centrosymmetric acceptors.[5,27,28] These factors collectively enable in-plane molecular rotations, often accompanied by significant changes in the atomic coordinates. In the field of semiconductors, studies on anthracene and **TCNQ** cocrystals have revealed that temperature-dependent phase transitions, driven by in-plane molecular motions of anthracene, can drastically alter the transfer characteristics of field-effect transistors (FETs), changing their behavior from n-type to ambipolar to p-type.[29] We have also contributed in this area, reporting the in-plane reorientation of halogenated acceptor fragments such as tetrafluoro-1,4-benzoquinone (**TFBQ**) and tetrafluoroterephthalonitrile in carbazole-derived cocrystals, which improved the photothermal conversion efficiency or changed the photoluminescence at low temperature.[30,31] Despite recent advancements, the development of CT cocrystals and the investigation of their possible internal molecular motions is still in progress, with scarce in-depth studies.

After carefully evaluating the information mentioned above, we designed two CT cocrystals based on indolo[3,2,1-*jk*]carbazole (**ICZ**) as a donor molecule. **ICZ** is a versatile molecule for CT cocrystals because its planar structure facilitates π-stacking, a crucial interaction for an efficient charge transfer process in cocrystals, but it has been barely used for this purpose. Electronically, **ICZ** may exhibit a duality, acting as either a donor or acceptor molecule, depending on its substituents.[32–45] Although planarization can diminish its donor strength by restricting the availability of the lone pair of electrons in the nitrogen towards pyrrole aromaticity,[41] this characteristic can be modulated by introducing large acceptor fragments into the structure. Several derivatives have been used in blue and green PhOLEDs,[33–35,38–40] dye-sensitized solar cells (DSSCs),[36,37] TADF emitters,[42,43,45] as hole-transporting material in perovskite solar cells,[46] and conducting films.[47] Given that its structure can be modified, large emission wavelengths and high quantum yields can be obtained,[32] facilitating the development of more efficient optoelectronic devices.

Considering that symmetrical molecules in CT cocrystals could exhibit in-plane motions, in this work, **ICZ** was cocrystallized with two acceptor molecules: 7,7,8,8-tetracyanoquinodimethane (**TCNQ**) and tetrafluoro-1,4-benzoquinone (**TFBQ**) (Fig. 1c). Single-crystal X-ray diffraction experiments and Fourier-transformed infrared spectroscopy data indicated that the cocrystal **ICZ-TCNQ** shows a stronger CT character, leading to a very broad UV-vis absorption. This cocrystal, when irradiated at 808 nm, shows a photothermal conversion efficiency (PTCE, η) of *ca.* 13%. Complementarily, variable-temperature single-crystal X-ray diffraction and calorimetric experiments showed that the **ICZ-TFBQ** cocrystal exhibits a phase transition at low temperatures with colossal thermal expansion, migrating to a higher-symmetry structure at 300 K, a phenomenon rarely observed in organic compounds. Solid-state nuclear magnetic resonance (ssNMR) experiments, through ^{19}F T_1 relaxation or ^{13}C CPMAS experiments, complemented with theoretical calculations, show that the **TFBQ** fragment undergoes very fast thermally-driven molecular motions, reaching hundreds of MHz at 348 K, with a rotational barrier of *ca.* 8 kcal mol^{-1}. The comparison between both cocrystals systems highlights the

structural and functional adaptability and versatility of **ICZ**, positioning it as a promising building block for multifunctional materials demonstrating the relevance of the choice of acceptor molecular could tailor the resulting properties, paving the way for novel applications.

Results and discussion

Synthesis and crystal structure of TCNQ and TFBQ cocrystals

The **ICZ** molecule was prepared through an adapted synthesis of the procedure reported by Hatta in 2021, as described in Scheme S1 (ESI†).[38] Single-crystal X-ray diffraction (SC-XRD) at 298 K of crystals grown from ethyl acetate revealed the crystal structure of the **ICZ** molecule in the orthorhombic space group $Pca2_1$ (Table S1, ESI†). The structural analysis showed a planar structure of the **ICZ** with a herringbone packing arrangement with CH···π and π–π interactions (Fig. S1a and b, ESI†). Furthermore, simultaneous differential scanning calorimetry and thermogravimetric analysis (DSC/TGA) revealed that the compound is stable until its decomposition temperature of 139 °C (Fig. S1c, ESI†). The calculated and experimental powder X-ray diffractograms showed a good agreement of the crystalline phase (Fig. S1d, ESI†). The coformers **TCNQ** and **TFBQ** were selected for cocrystallization as acceptor moieties due to their ability to establish intermolecular CT states with donor molecules.[48–53] Cocrystals **ICZ-TCNQ** and **ICZ-TFBQ** were obtained as solvent-free forms from an equimolar solution of the compounds in acetone, as is detailed in the ESI.† SC-XRD enabled us to obtain the crystal structures in a monoclinic $P2_1/n$ and *Pbcn* space groups, respectively (Tables S4 and S9, ESI†), both at 300 K.

Both **ICZ-TCNQ** and **ICZ-TFBQ** cocrystals exhibit 1 : 1 stoichiometry with mixed donor–acceptor (D/A) stacking. **ICZ-TCNQ** and **ICZ-TFBQ** crystallize with predominant π–π interactions between D/A centroids with distances of 3.328 and 3.348 Å, respectively (Fig. 2a). The structure of **ICZ-TCNQ** is stabilized by weak hydrogen bonds involving the cyano groups of **TCNQ** and neighboring **ICZ** molecules. Additionally, C–H···N interactions between adjacent **TCNQ** molecules promote a zigzag arrangement (Fig. 2b). On the other hand, **ICZ-TFBQ** crystallizes with a herringbone packing arrangement due to the presence of hydrogen bonds, including C–H···O and C–H···F interactions between **TFBQ** and **ICZ** molecules that further stabilize the crystal structure (Fig. 2c). Moreover, the **TFBQ** molecules exhibit disorder at 300 K. In both cases, the cooperative effect of π interactions and the hydrogen bonds play a crucial role in holding the molecules together within the cocrystals.

Coupled DSC and TGA analysis confirmed thermal stability for the cocrystals up to 240 °C for **ICZ-TCNQ** and 180 °C for **ICZ-TFBQ**, with no phase transitions observed in the range from 25 to 450 °C (Fig. S2, ESI†) prior the melting point of the cocrystals, immediately followed by their decomposition, as evidenced by the loss of **TCNQ** and **TFBQ** molecules. For further analysis, large amounts of each cocrystal were prepared and ground. PXRDs of both cocrystals revealed excellent agreement between the calculated and experimental diffractograms (Fig. S3, ESI†).

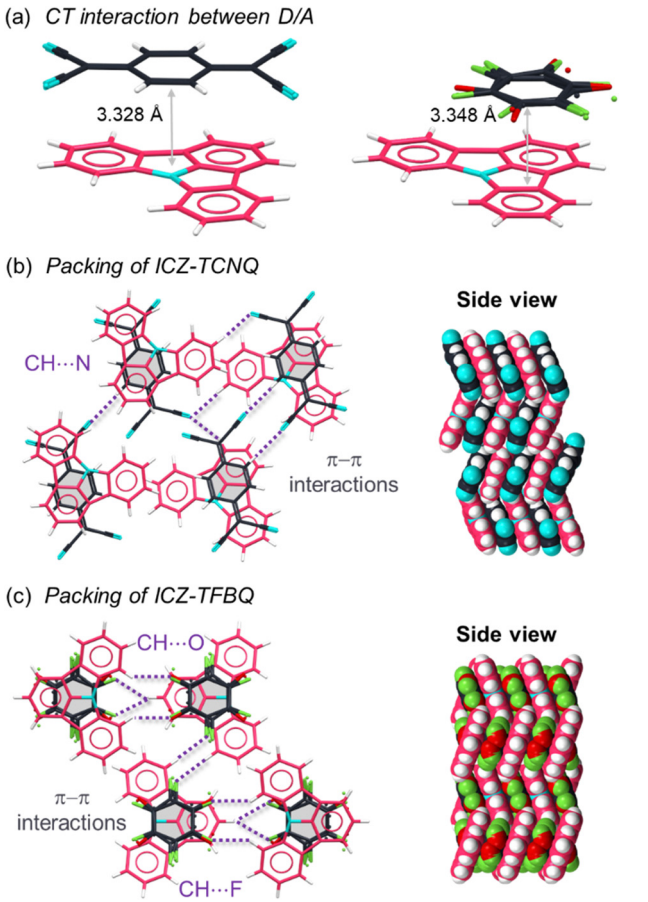

Fig. 2 (a) Interplanar distances between donor and acceptor molecules in **ICZ-TCNQ** (left) and **ICZ-TFBQ** (right). Intermolecular π–π (grey) and hydrogen bond (purple) interactions in (b) **ICZ-TCNQ** cocrystal and (c) **ICZ-TFBQ** cocrystal with their respective packing.

Characterization of the intermolecular CT character of cocrystals

The growth of **TCNQ** and **TFBQ** cocrystals yielded black crystals with block morphology, which is a characteristic typically associated with the presence of CT processes between the D/A dyads. To further explore this feature, complementary techniques such as solid-state UV-vis absorption spectroscopy, through diffuse reflectance technique, at room temperature was employed (Fig. 3a). While the coformers **ICZ**, **TCNQ** and **TFBQ** display absorption maxima at 384, 458, and 401 nm, respectively, cocrystals exhibit much broader absorption bands.

For **ICZ-TFBQ**, the resulting band extends up to 750 nm. In contrast, **ICZ-TCNQ** shows absorption in the near-infrared region extended slightly further than 800 nm. Based on this data, we used the Kubelka–Munk function to obtain the direct E_g, which was determined by plotting the reflectance $F(R)$ as a function of the energy $h\nu$, employing a modified Tauc plot.[54] The crossing of the linear portions with the *x*-axis determined

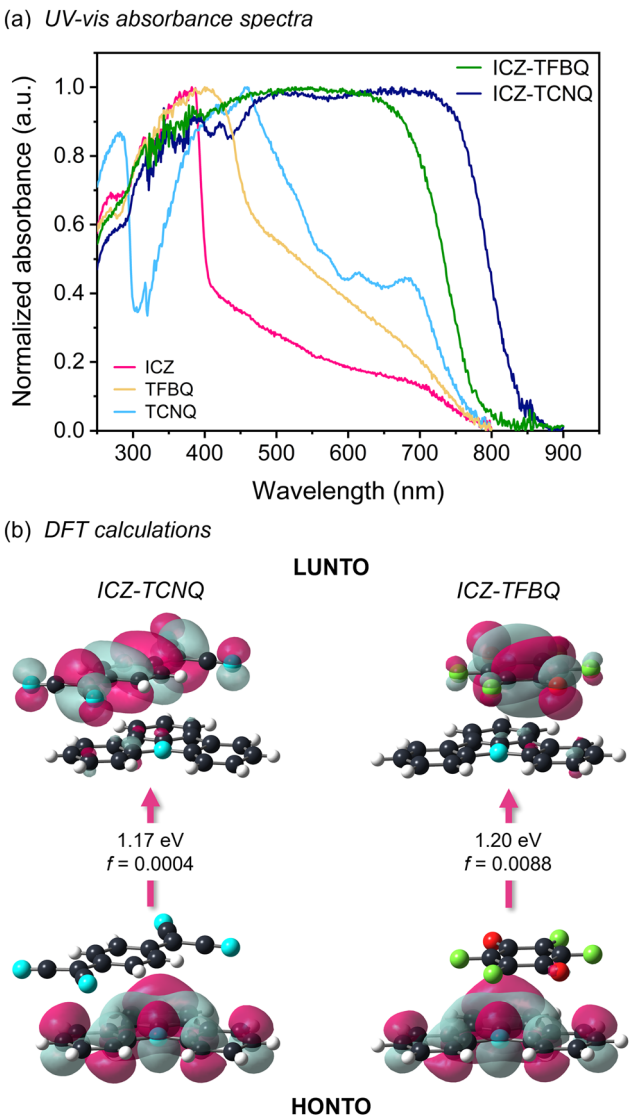

Fig. 3 (a) Solid-state UV-vis absorbance spectra of starting materials and cocrystals. (b) Natural transition orbitals (NTOs) of **ICZ-TCNQ** (left) and **ICZ-TFBQ** (right) using TDDFT with the CAM-B3LYP functional at the 6-311+G(d,p) level of theory. The associated energies (in eV) and oscillator strengths (*f*) are included.

the E_g of the cocrystals, being 1.50 and 1.62 eV for **ICZ-TCNQ** and **ICZ-TFBQ**, respectively (Fig. S4, ESI†).

Fourier-transform infrared experiments (FTIR) helped us better understand the intermolecular CT phenomenon. It is well-established that shifts in the wavenumber values of vibrational modes, such as the stretching frequencies of the cyano and carbonyl groups, reflect changes in the electronic environment during the CT process.[55–61] Based on FTIR data, it was possible to determine the degree of charge transfer (DCT) in the cocrystals, as shown in the ESI.† Specifically, Fig. S5a (ESI†) shows a shift of 6 cm^{-1} in the cyano-stretching frequency of **TCNQ**, from 2221 cm^{-1} in the pristine material to 2215 cm^{-1} in the **ICZ-TCNQ** cocrystal. Similarly, Fig. S5b (ESI†) shows a 9 cm^{-1} shift in the carbonyl stretching frequency of **TFBQ**, from 1669 cm^{-1} to 1660 cm^{-1} upon cocrystallization with **ICZ**. These frequency shifts helped us to calculate that DCT values for each cocrystal are 0.27 and 0.06 for **ICZ-TCNQ** and **ICZ-TFBQ**, respectively, presented in Table S2 (ESI†). The calculation of the energy frameworks at 300 K further confirmed the lower DCT value observed for the cocrystal with **TFBQ**. These were performed using CrystalExplorer 21[62] with the CE-B3LYP/6-31G(d,p) functional, included in the software. The calculations yield total energies in the cocrystals between **ICZ** and coformers of *ca.* −60 kJ mol^{-1} for **ICZ-TCNQ** and −47 kJ mol^{-1} for **ICZ-TFBQ**, as shown in Fig. S6 and S7 (ESI†), respectively.

Moreover, to study the electronic transitions in D/A pairs, the dimers of each cocrystal were geometrically optimized, using the crystallographic coordinates from SC-XRD structures at 300 K with the Perdew–Burke–Ernzerhof (PBE0)[63] functional at the 6-311G(d,p) level, included in Gaussian09.[64] Afterward, the energies of the natural transition orbitals (NTOs) in the cocrystals were calculated using time-dependent density functional theory (TD-DFT) with the CAM-B3LYP[65]/6-311+G(d,p) functional, and the Grimme's D3-dispersion correction approach.[66] It was observed that the lowest unoccupied NTO (LUNTO) orbitals for both **ICZ-TCNQ** and **ICZ-TFBQ** dyads are localized over the respective acceptor fragments (Fig. 3b). In contrast, the highest occupied NTO (HONTO) orbitals are located over the **ICZ** molecule for both cases. Moreover, the energy gaps for the first excited state correspond to a $^1CT_1$, with 1.17 and 1.20 eV for **ICZ-TCNQ** and **ICZ-TFBQ**, respectively. These values are significantly smaller than the energy gaps calculated for the starting materials (Fig. S8, ESI†). The oscillator strengths calculated for both systems are small and close to zero, which is a typical case for intermolecular CT transitions due to the weak overlap of orbitals through space. The small energy gaps and thermal stability, supported by both experimental and computational results, suggest the potential application of these crystalline solids in semiconducting devices.[67]

Considering the spectroscopic and optical data presented above, we also investigated the potential photothermal conversion (PTC) properties of both cocrystals. As detailed in the ESI,† each cocrystal was irradiated with an 808 nm IR laser. The temperature change of the solids upon irradiation was recorded using an IR thermal camera (Fig. 4a). The PTC efficiency (PTCE) was calculated using eqn (1).

$$\eta = \frac{hS\Delta T_{max}}{I(1-10^{-A_\lambda})} \quad (1)$$

where η is the PTC efficiency, h is the heat transfer coefficient, S is the surface area, ΔT_{max} is the maximum change in the temperature, I is the power density of the laser, and A_λ is the absorbance of the cocrystals at the laser wavelength. As a reference, the heating curves of a blank exhibited only a slight temperature increase of 1.9 °C (Fig. S9a, ESI†).

Due to the limitation to a single irradiation wavelength (808 nm) of the laser in our setup, and despite the broad absorption exhibited by **ICZ-TFBQ** (Fig. S9b, ESI†), we were unable to measure significant temperature changes upon the irradiation of this cocrystal (Fig. S11, ESI†). Conversely, **ICZ-TCNQ** exhibited a PTCE of 12.8 ± 2.1% at an irradiation

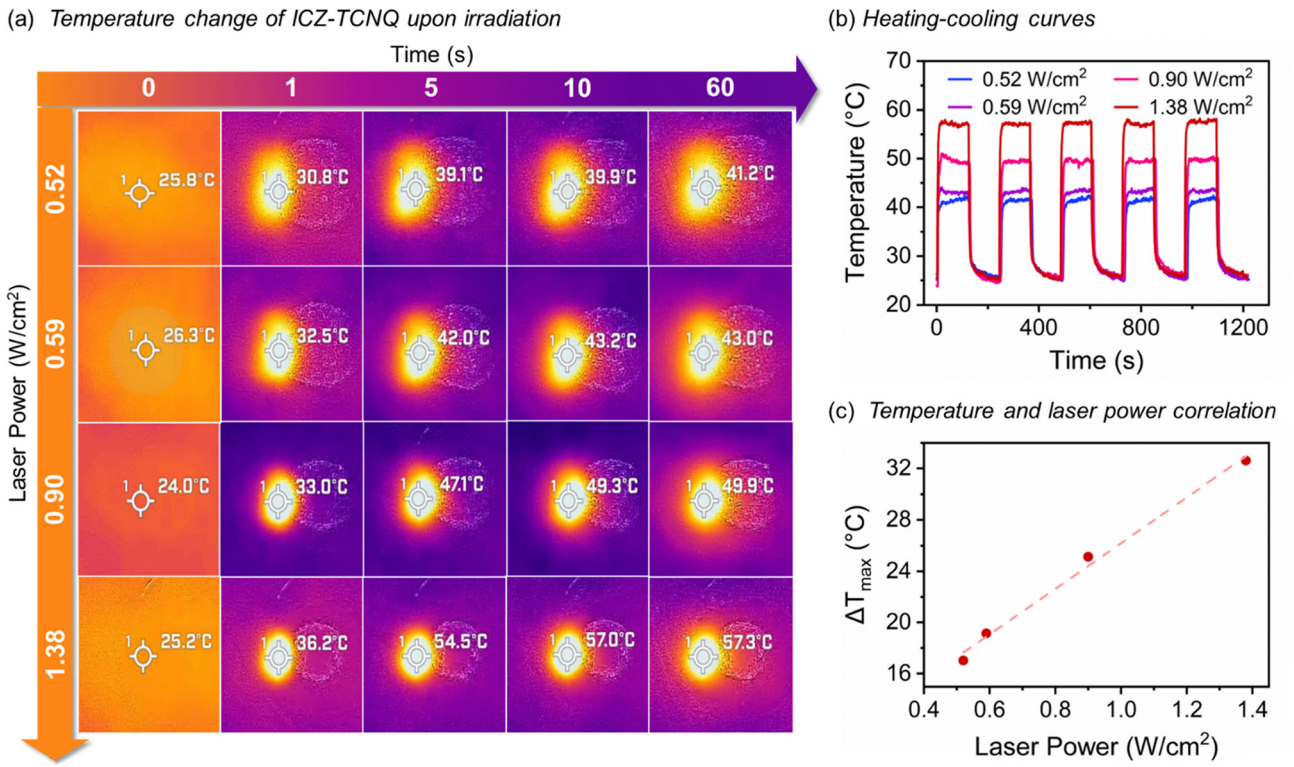

Fig. 4 (a) Thermal IR images of **ICZ-TCNQ** under heating at different times and density power. (b) Heating–cooling curves for **ICZ-TCNQ**. (c) Linear relationship between change in temperature and the applied laser power.

intensity of 0.52 W cm^{-2}. Upon variation of the irradiation power density, the maximum temperature achieved in samples of **ICZ-TCNQ** changed progressively, as shown in Fig. 4b. Moreover, a linear relationship between temperature change and the applied laser power was demonstrated, as depicted in Fig. 4c. To ensure the stability of the crystalline phase after the PTC measurements, the experimental PXRD diffractogram is depicted in Fig. S12 (ESI†) and compared with the diffractogram obtained before the irradiation cycles, it displays a good agreement.

Phase transition and thermal expansion of ICZ-TFBQ through variable-temperature SC-XRD

Over time, our group has developed an increasing interest in investigating molecular motions within crystalline materials and their possible association with other properties, *e.g.* the thermosalient effect,[68] or the luminescent behavior,[69] among others.[70] Due to its molecular size and symmetry, **TFBQ** has been a pivotal molecule for studying these phenomena in cocrystals and its diffusion in metal–organic frameworks (MOFs).[30,71]

Driven by the observation of disorder of the **TFBQ** molecule in the **ICZ-TFBQ** cocrystal at 298 K, we conducted variable-temperature single-crystal X-ray diffraction (VT-SCXRD) studies from 100 K to 300 K. Additionally, these studies helped us identify a phase transition at low temperatures. It is important to note that the **TCNQ**-based cocrystal did not undergo any structural change throughout the temperature interval, showing only a subtle elongation of the anisotropic displacement parameters (ADPs) (Fig. S14, ESI†).

In sharp contrast, **ICZ-TFBQ** exhibited a translationengleiche phase transition, showing a $P2_1/c$ space group at 100 K with ordered **TFBQ** molecules, compared to a *Pbcn* space group at 300 K, with **TFBQ** molecules significantly disordered (Fig. 5a) and involving an increase in the symmetry. DSC measurements from 300 K to 200 K displayed an exothermal process at *ca.* 281 K, which corresponded to the single-crystal to single-crystal (SCSC) phase transition from the low-temperature (LTP) to the high-temperature (HTP) phase (Fig. S15a, ESI†). This transition is characterized by a prominent change in the angle between the aromatic cores within the herringbone packing, with a gradual adjustment of the atomic positions of the **TFBQ** (Fig. 5b) and a reorientation of the crystallographic axes, resulting in an exchange of unit cell dimensions due to the new constraints in the *Pbcn* space group.

Notably, when **ICZ-TFBQ** was heated from 200 to 300 K, a continuous increase in the unit cell volume was observed, from 1755.76 to 1846.85 $Å^3$ as depicted in Fig. S15b (ESI†). Furthermore, the **TFBQ** molecule took four distinct orientations within the unit cell, each with a site occupation factor of 25%. Based on the classification of phase transitions proposed by Christian,[72] these structural changes are indicative of a second-order martensitic transition. This type of transition is characterized by continuous and concerted displacements/rotations of all molecules within the crystal lattice, accompanied by a gradual change in volume.[73] While second-order martensitic

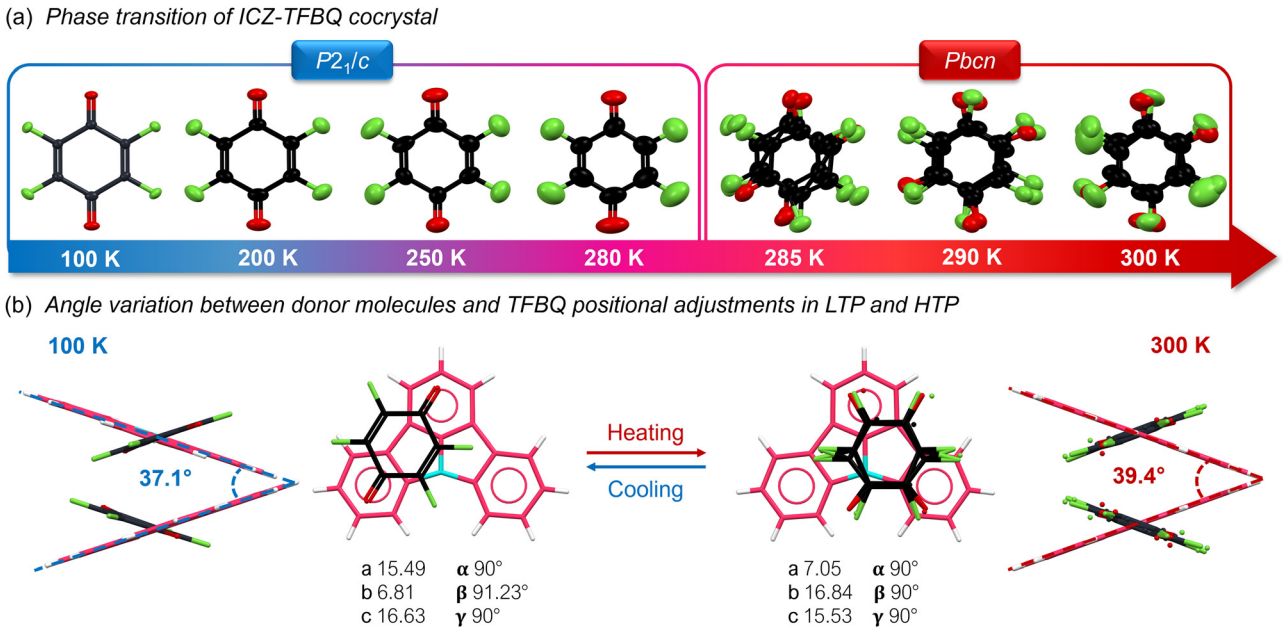

Fig. 5 Molecular structure differences between the LTP and HTP polymorphs in **ICZ-TFBQ**. (a) Phase transition from ordered to disordered **TFBQ** molecules depending on temperature. (b) Changes of the packing angles of the aromatic donor cores of **ICZ-TFBQ** from LTP to HTP and displacement of the atomic positions of the **TFBQ**.

transitions are relatively rare in organic crystals, their occurrence offers valuable insights into the intricate relationship between molecular structure and the macroscopic properties of the material.

The strength of the intermolecular interactions can be affected by temperature, strong interactions are recognized to be less affected by the temperature than weaker ones. To gain deeper insight into the differences in the strength of interaction between the two cocrystals, we determined their thermal expansion parameters. Thermal expansion (TE) is the fundamental property of solids that modify their dimensions due to an increase in temperature. The magnitude of this parameter closely depends on the crystal packing, intermolecular interactions, and the type of atoms of the constituent molecules.[74,75] TE can be categorized as positive (PTE), negative (NTE), or zero (ZTE), if the solid increases, decreases, or its dimensions remain unchanged with rising temperature.

Using the VT SC-XRD data, we calculated the TE coefficients a_{x1}, a_{x2}, a_{x3} along the three principal directions and expansivity indicatrices employing the software Pascal,[76] depicts an example that uses the unit cell parameters at variable temperatures. For **ICZ-TCNQ**, we employed SC-XRD data from 100 to 300 K, whereas for **ICZ-TFBQ**, we calculated the LTP TE coefficients in the range from 200 to 280 K.

The results suggest that thermal expansion of **ICZ-TCNQ** is anisotropic along the three principal directions. The value of a_{x1} is 17 MK^{-1}, coinciding with crystallographic *a*-axis, a_{x2} was calculated as 75 MK^{-1}, with an approximate direction along the *c*-axis. Moreover, the larger thermal expansion occurs along the direction of the D/A π-stacking, with a calculated value of *ca.* 78 MK^{-1} (Fig. S16, ESI†).

On the other hand, the **ICZ-TFBQ** showed substantially different anisotropic TE behavior, as observed in Fig. 6. The a_{x1} exhibited an NTE value of −60 MK^{-1}, corresponding to the direction of edge-to-edge interactions between contiguous molecules of **ICZ** and **TFBQ** located along the *ab* plane (Fig. S17, ESI†). The a_{x2} value is 95 MK^{-1}, in the opposite direction of a_{x1}. Finally, a_{x3} aligns with the crystallographic *b*-axis, matching the direction of the π-stacking between **ICZ** and **TFBQ**, with a calculated value of 206 MK^{-1} (Fig. 6b). As result of this thermal expansion, the π-stacking calculated using the centroid of **TFBQ** and the plane formed by **ICZ** distances increases at high temperature. Since two distinct **ICZ-TFBQ**

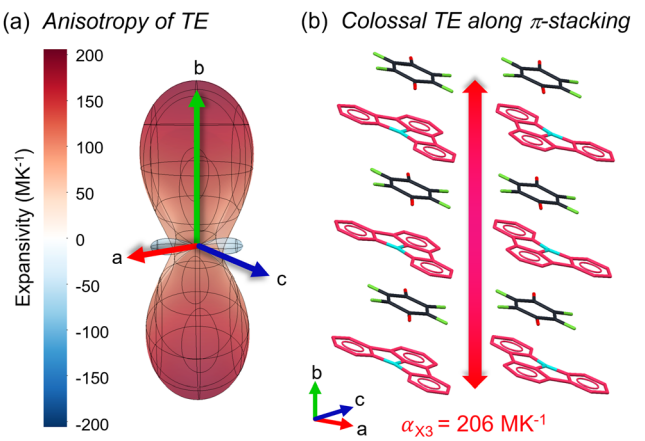

Fig. 6 (a) Expansivity indicatrix for **ICZ-TFBQ**. (b) Crystalline packing of **ICZ-TFBQ** seen along the *b*-axis in the direction of the π-stacking between D/A molecules. The TE coefficient is displayed and illustrated with red arrows.

stacking distances are present in the cocrystal, both were measured and plotted. For example, at 200 K the two distances (*D*1, *D*2) are 3.215 Å and 3.314 Å, but at 280 K the distances are 3.277 Å and 3.355 Å, as shown in Fig. S18 (ESI†). TE coefficients larger than 100 MK^{-1} are classified as colossal, and in this cocrystal, is *ca.* 2.6 times larger than that found in **ICZ-TCNQ**.[77,78]

Thermally-driven rotational motions of TFBQ through ssNMR and DFT calculations

As temperature increases, the progressive elongation of the ADPs of the **TFBQ** in the collected VT SC-XRD structures could be indicative of in-plane reorientations. To confirm this hypothesis, solid-state ^{13}C NMR experiments were performed using the cross-polarization magic angle spinning (CPMAS) technique from 249 to 343 K. Analysis of the signals of the carbonyl and aromatic carbons in **TFBQ** revealed small but noticeable variations in their chemical shifts, suggesting changes in the magnetic environment of these nuclei dependent on the temperature (Fig. 7a).

To provide further insight, ^{19}F T_1 relaxation experiments were performed using a saturation-recovery pulse sequence from 173 (the minimum temperature available in the spectrometer) to 348 K. T_1 is a parameter that provides crucial information about the dissipation of energy from spin in nuclei to the lattice (spin–lattice relaxation) due to the application of a radiofrequency pulse, which can provide insights on molecular motions as a relaxation mechanism.

For thermally-driven motions, the T_1 relaxation times follow an Arrhenius-type function, from which the associated energy barriers for rotation (E_a) for the dynamic processes involved in the crystal lattice can be obtained.[79] The results presented in Fig. 7b show a decrease in T_1 relaxation times with increasing temperature, which is indicative of increasing molecular mobility as an additional relaxation pathway. These experimental observations, along with previous studies of the **TFBQ** dynamics,[30] suggest that this fragment rotates at frequencies of hundreds of MHz at *ca.* 348 K. Analysis of the relaxation data by a linear Arrhenius fit yielded E_a of 7.98 kcal mol^{-1} associated with the fast reorientational motion of **TFBQ**. The T_1 times measured from 248 up to 348 K, corresponding to the HTP, display fair linear behavior (R^2 = 0.9455). Conversely, the T_1 times corresponding to the LTP ($T < 223$ K) do not align with the previously observed trend, indicating a different dynamic process arising at lower temperatures.

To further support the presence of molecular motions in **ICZ-TFBQ**, DFT calculations were performed to estimate the rotational energy profile of the **TFBQ** at 100 and 300 K for the LTP and HTP, respectively. Initially, we carried out periodic DFT energy calculations on the LTP and HTP phases of **ICZ-TFBQ** by manually rotating the **TFBQ** molecule within the plane in 10° increments (Fig. S19, ESI†). These rotational energy profiles, obtained without performing geometry optimization at each step, represent upper-bound estimates of the rotational barriers. In practice, these barriers are likely to be lower, as molecular geometries can relax to accommodate rotation. To further investigate the rotational states and associated energy barriers, we extracted molecular clusters from the crystal structures, each consisting of a central **TFBQ** molecule surrounded by neighboring **ICZ** molecules. We then optimized the geometries corresponding to the global minimum, the two local minima near ±60°, and the transition states connecting these local minima to the global minimum, employing the B3LYP functional. During these optimizations, the geometries of the surrounding **ICZ** molecules were fixed, while only the central **TFBQ** molecule was allowed to relax.

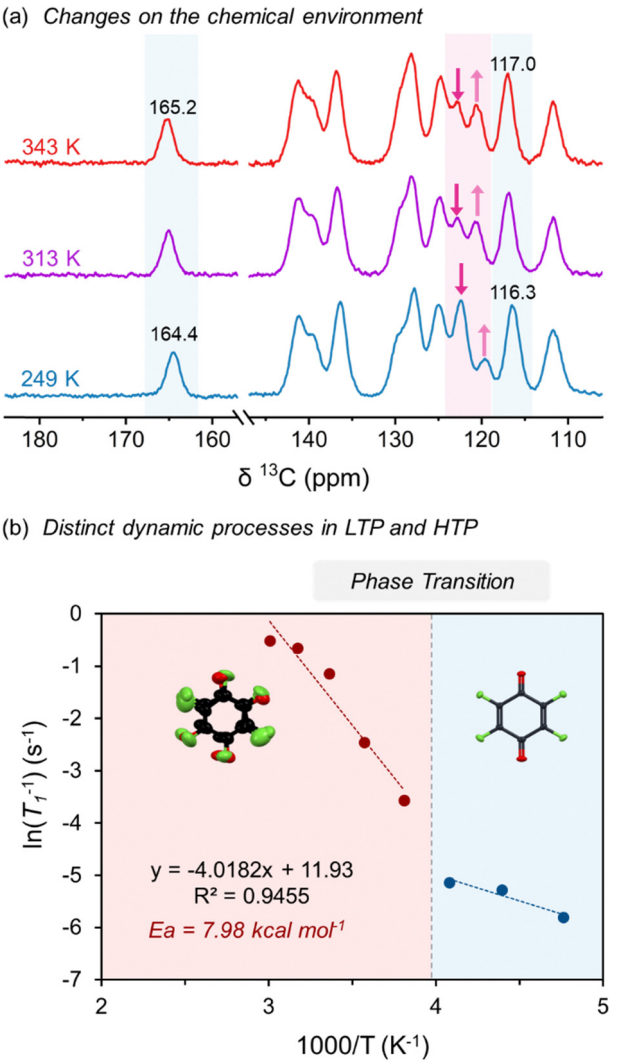

Fig. 7 (a) ^{13}C CPMAS spectra of **ICZ-TFBQ** at three different temperatures. (b) Arrhenius fitting of the ^{19}F T_1 relaxation times obtained from saturation recovery experiments.

The energy profile, illustrated in Fig. 8a, revealed two local minima at −60° and +60° relative to the global minimum at 0° with relative energies of *ca.* 3.0 and 0.2 kcal mol^{-1} at 100 and 300 K, respectively. To achieve these trajectories, the activation energies for rotation were calculated as 8.1 kcal mol^{-1} for HTP and *ca.* 14.0 kcal mol^{-1} for the LTP. These values indicate that **TFBQ** undergoes in-plane rotations of 60° (Fig. 8b), supporting the experimental data which suggests that the motion of **TFBQ**

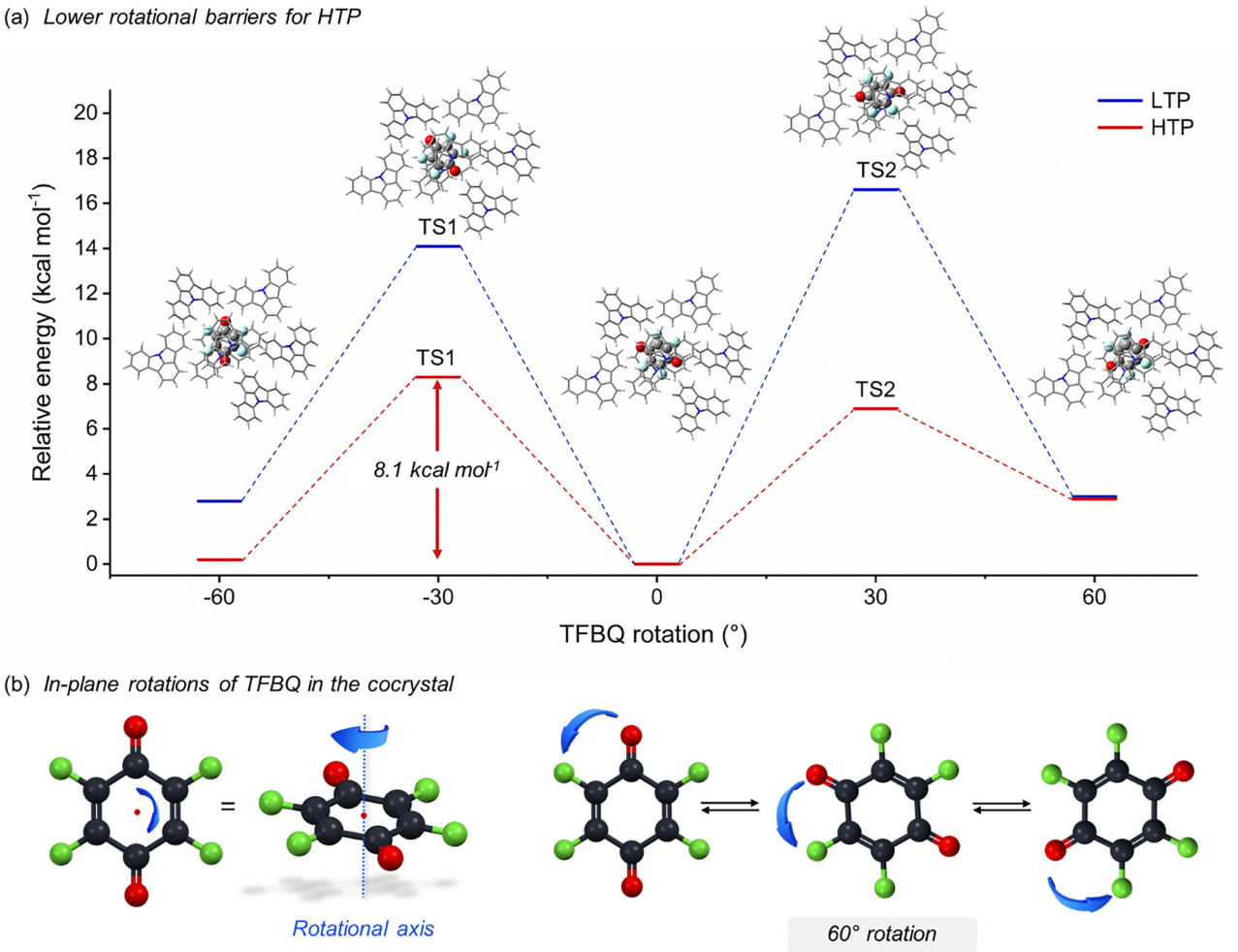

Fig. 8 (a) Energetic profile of the 60° rotations of **TFBQ** fragment in the cocrystal. (b) Illustration of the 6-fold motion experiencing by the **TFBQ** fragment.

fragment is favored at 300 K. From these results, it can be postulated that the fast internal motion of the acceptor component in this cocrystal could benefit the PTC properties when measured under appropriate experimental conditions.

Conclusions

Through a series of spectroscopic techniques, theoretical calculations, and PTC measurements, we have successfully unveiled the performance of two indolocarbazole-based CT cocrystals, exhibiting charge transfer. Notably, it was demonstrated that **ICZ-TCNQ** portrays a photothermal conversion efficiency of *ca.* 13%. Although PTC properties were not measurable for the **TFBQ** cocrystal, it exhibited a distinct low-temperature phase transition at *ca.* 281 K resulting in a higher symmetry structure at 300 K, accompanied by a NTE of -60 MK^{-1} and a colossal PTE of 206 MK^{-1}. This transition is characterized by the **TFBQ** fragment undergoing fast thermally-driven in-plane molecular rotations with frequencies of hundreds of MHz at *ca.* 348 K. These molecular rotations were elucidated by T_1 relaxation measurements with an activation energy of 7.9 kcal mol^{-1} and further supported by DFT calculations. Future studies of the **TFBQ**-based cocrystal will shine light on the impact of these rotations on the possible PTC properties. This comparative analysis of **ICZ-TCNQ** and **ICZ-TFBQ** emphasize the functional adaptability of **ICZ**-based cocrystals. The combination of efficient PTC properties and dynamic molecular motion illustrates how tuning CT interactions enables access to diverse and complementary material functionalities. Together, these findings highlight the versatility and potential of **ICZ**-based CT cocrystals in multifunctional material design.

Data availability

The data supporting this article has been included as part of the ESI.† Further information can be provided upon reasonable request.

Conflicts of interest

The authors declare no competing interests.

Acknowledgements

This work was supported by DGAPA PAPIIT IN212625 and CONACHYT Ciencia de Frontera 1715644. J. C. thanks CONAHCYT for a MSc scholarship (1341078). E. H.-M. and A. N.-H. thank CONAHCYT for a PhD scholarship (1078913 and 957838). We acknowledge the technical assistance from M. C. García González PhD and F. J. Pérez Flores PhD (MS), E. Huerta Salazar MSc, I. Chávez PhD, R. Gaviño PhD, B. Quiroz PhD and M. A. Peña González BSc (solution NMR), M. E. García Aguilera PhD (ssNMR), A. Núñez Pineda MSc (DSC/TGA), U. Hernández Balderas PhD and M. Tapia Tapia MSc (PXRD), D. Martínez Otero PhD (SC-XRD), A. Romo-Pérez PhD (FTIR), Virginia Gómez Vidales MSc (ESR), M. P. Orta Pérez BSc (combustion analysis) and Mario Rodríguez PhD (ssUV-Vis). We are also thankful for computing time LANCAD-UNAM-DGTIC-392. This work was supported by the Ministry of Education, Youth and Sports of the Czech Republic through the Inter-COST program (ID: LUC24101). This research used resources of the Advanced Light Source, which is a DOE Office of Science User Facility under contract no. DE-AC02-05CH11231.

References

1 W. Zhu, X. Zhang and W. Hu, Molecular Cocrystal Odyssey to Unconventional Electronics and Photonics, *Sci. Bull.*, 2021, **66**(5), 512–520, DOI: **10.1016/j.scib.2020.07.034**.

2 H. S. Kim, J. Y. Koo and H. C. Choi, Selective Reduction Approach in Cocrystal Systems for Highly Conducting Organic Radical Crystals, *Chem. Mater.*, 2023, **35**(4), 1762–1768, DOI: **10.1021/acs.chemmater.2c03622**.

3 Y. Qin, J. Zhang, X. Zheng, H. Geng, G. Zhao, W. Xu, W. Hu, Z. Shuai and D. Zhu, Charge-Transfer Complex Crystal Based on Extended-π-Conjugated Acceptor and Sulfur-Bridged Annulene: Charge-Transfer Interaction and Remarkable High Ambipolar Transport Characteristics, *Adv. Mater.*, 2014, **26**(24), 4093–4099, DOI: **10.1002/adma.201400056**.

4 R. A. Wiscons, N. R. Goud, J. T. Damron and A. J. Matzger, Room-Temperature Ferroelectricity in an Organic Cocrystal, *Angew. Chem., Int. Ed.*, 2018, **57**(29), 9044–9047, DOI: **10.1002/anie.201805071**.

5 J. Harada, M. Ohtani, Y. Takahashi and T. Inabe, Molecular Motion, Dielectric Response, and Phase Transition of Charge-Transfer Crystals: Acquired Dynamic and Dielectric Properties of Polar Molecules in Crystals, *J. Am. Chem. Soc.*, 2015, **137**(13), 4477–4486, DOI: **10.1021/jacs.5b00412**.

6 D. Barman, M. Annadhasan, A. P. Bidkar, P. Rajamalli, D. Barman, S. S. Ghosh, R. Chandrasekar and P. K. Iyer, Highly Efficient Color-Tunable Organic Co-Crystals Unveiling Polymorphism, Isomerism, Delayed Fluorescence for Optical Waveguides and Cell-Imaging, *Nat. Commun.*, 2023, **14**(1), 6648, DOI: **10.1038/s41467-023-42017-8**.

7 S. Kassem, T. van Leeuwen, A. S. Lubbe, M. R. Wilson, B. L. Feringa and D. A. Leigh, Artificial Molecular Motors, *Chem. Soc. Rev.*, 2017, **46**(9), 2592–2621, DOI: **10.1039/C7CS00245A**.

8 J. Groppi, M. Baroncini, M. Venturi, S. Silvi and A. Credi, Design of Photo-Activated Molecular Machines: Highlights from the Past Ten Years, *Chem. Commun.*, 2019, **55**(84), 12595–12602, DOI: **10.1039/C9CC06516D**.

9 L. Catalano and P. Naumov, Exploiting Rotational Motion in Molecular Crystals, *CrystEngComm*, 2018, **20**(39), 5872–5883, DOI: **10.1039/C8CE00420J**.

10 M. Schliwa and G. Woehlke, Molecular Motors, *Nature*, 2003, **422**(6933), 759–765, DOI: **10.1038/nature01601**.

11 R. D. Vale, The Molecular Motor Toolbox for Intracellular Transport, *Cell*, 2003, **112**(4), 467–480, DOI: **10.1016/S0092-8674(03)00111-9**.

12 S. Erbas-Cakmak, D. A. Leigh, C. T. McTernan and A. L. Nussbaumer, Artificial Molecular Machines, *Chem. Rev.*, 2015, **115**(18), 10081–10206, DOI: **10.1021/acs.chemrev.5b00146**.

13 L. A. Amos, Molecular Motors: Not Quite like Clockwork, *Cell. Mol. Life Sci.*, 2008, **65**(4), 509–515, DOI: **10.1007/s00018-008-7518-3**.

14 G. S. Kottas, L. I. Clarke, D. Horinek and J. Michl, Artificial Molecular Rotors, *Chem. Rev.*, 2005, **105**(4), 1281–1376, DOI: **10.1021/cr0300993**.

15 I. Liepuoniute, M. J. Jellen and M. A. Garcia-Garibay, Correlated Motion and Mechanical Gearing in Amphidynamic Crystalline Molecular Machines, *Chem. Sci.*, 2020, **11**(48), 12994–13007, DOI: **10.1039/D0SC04495D**.

16 A. Navarro-Huerta, M. J. Jellen, J. Arcudia, S. J. Teat, R. A. Toscano, G. Merino and B. Rodríguez-Molina, Tailoring the Cavities of Hydrogen-Bonded Amphidynamic Crystals Using Weak Contacts: Towards Faster Molecular Machines, *Chem. Sci.*, 2021, **12**(6), 2181–2188, DOI: **10.1039/D0SC05899H**.

17 Z. Liu, Y. Wang and M. A. Garcia-Garibay, Rotational Dynamics of an Amphidynamic Zirconium Metal–Organic Framework Determined by Dielectric Spectroscopy, *J. Phys. Chem. Lett.*, 2021, **12**(24), 5644–5648, DOI: **10.1021/acs.jpclett.1c01333**.

18 M. C. Mayorquín-Torres, A. Colin-Molina, S. Pérez-Estrada, A. Galano, B. Rodríguez-Molina and M. A. Iglesias-Arteaga, Synthesis, Characterization, and Solid State Dynamic Studies of a Hydrogen Bond-Hindered Steroidal Molecular Rotor with a Flexible Axis, *J. Org. Chem.*, 2018, **83**(7), 3768–3779, DOI: **10.1021/acs.joc.8b00134**.

19 B. P. Mali, S. R. Dash, M. Annadhasan, A. Biswas, K. Manoj, K. Vanka and R. G. Gonnade, Cocrystal Approach to Modulate the Photoluminescent Properties of a GFP Chromophore Analogue: Role of Halogen/Hydrogen Bonding in Achieving a Wide Range of Solid-State Fluorescence Emissions, *Cryst. Growth Des.*, 2023, **23**(7), 5052–5065, DOI: **10.1021/acs.cgd.3c00307**.

20 A. A. Dar and S. Rashid, Organic Co-Crystal Semiconductors: A Crystal Engineering Perspective, *CrystEngComm*, 2021, **23**(46), 8007–8026, DOI: **10.1039/D1CE01117K**.

21 Y. Yu, X.-Y. Xia, C.-F. Xu, Z.-J. Lv, X.-D. Wang and L.-S. Liao, Customizable Organic Charge-Transfer Cocrystals for the

Dual-Mode Optoelectronics in the NIR (II) Window, *J. Am. Chem. Soc.*, 2024, **146**(17), 11845–11854, DOI: **10.1021/jacs.4c00648**.

22 S. Zhao, J.-X. Zhang, C.-F. Xu, Y. Ma, J.-H. Luo, H. Lin, Y. Shi, X.-D. Wang and L.-S. Liao, Programmable In-Situ Co-Assembly of Organic Multi-Block Nanowires for Cascade Optical Waveguides, *Angew. Chem., Int. Ed.*, 2024, **63**(52), e202412712, DOI: **10.1002/anie.202412712**.

23 B. Wu, M.-P. Zhuo, Y.-L. Shi, L.-F. Gu, Y.-D. Zhao, Y. Su, Y.-Y. Li, H. Lu, W.-F. Li, Z.-S. Wang and X.-D. Wang, Directional Self-Assembly of Organic Semi-Type Core-Shell Microwires for Programmable Visible-to-near-Infrared Waveguiding Conversion, *Chem*, 2025, 102497, DOI: **10.1016/j.chempr.2025.102497**.

24 Y.-T. Chen, W. Chen, J. He, G. Zhang, X. Wen, S. Ran, Z. Deng, S. Zhu, H. Li, S. Ni, S. Chen, L. Dang and M.-D. Li, Tailormade Nonradiative Rotation Tuning of the Near-Infrared Photothermal Conversion in Donor–Acceptor Cocrystals, *J. Phys. Chem. C*, 2021, **125**(46), 25462–25469, DOI: **10.1021/acs.jpcc.1c09151**.

25 J.-C. Liu, T. Li, H. Yu, J. Y. Huang, P.-X. Li, Z.-Y. Ruan, P.-Y. Liao, C. Ou, Y. Feng and M.-L. Tong, Integrating Molecular Motions in Ternary Cocrystals for NIR-II Photothermal Conversion, *Angew. Chem., Int. Ed.*, 2025, **64**(1), e202413805, DOI: **10.1002/anie.202413805**.

26 S. Bracco, T. Miyano, M. Negroni, I. Bassanetti, L. Marchio', P. Sozzani, N. Tohnai and A. Comotti, CO2 Regulates Molecular Rotor Dynamics in Porous Materials, *Chem. Commun.*, 2017, **53**(55), 7776–7779, DOI: **10.1039/C7CC02983G**.

27 J. Harada, N. Yoneyama, S. Sato, Y. Takahashi and T. Inabe, Crystals of Charge-Transfer Complexes with Reorienting Polar Molecules: Dielectric Properties and Order–Disorder Phase Transitions, *Cryst. Growth Des.*, 2019, **19**(1), 291–299, DOI: **10.1021/acs.cgd.8b01418**.

28 R. Bhowal, A. A. Balaraman, M. Ghosh, S. Dutta, K. K. Dey and D. Chopra, Probing Atomistic Behavior To Unravel Dielectric Phenomena in Charge Transfer Cocrystals, *J. Am. Chem. Soc.*, 2021, **143**(2), 1024–1037, DOI: **10.1021/jacs.0c11459**.

29 S. Yokokura, Y. Takahashi, H. Nonaka, H. Hasegawa, J. Harada, T. Inabe, R. Kumai, H. Okamoto, M. M. Matsushita and K. Awaga, Switching of Transfer Characteristics of an Organic Field-Effect Transistor by Phase Transitions: Sensitive Response to Molecular Dynamics and Charge Fluctuation, *Chem. Mater.*, 2015, **27**(12), 4441–4449, DOI: **10.1021/acs.chemmater.5b01383**.

30 A. Navarro-Huerta, D. A. Hall, J. Blahut, V. Gómez-Vidales, S. J. Teat, J. M. Marmolejo-Tejada, M. Dračínský, M. A. Mosquera and B. Rodríguez-Molina, Influence of Internal Molecular Motions in the Photothermal Conversion Effect of Charge-Transfer Cocrystals, *Chem. Mater.*, 2023, **35**(23), 10009–10017, DOI: **10.1021/acs.chemmater.3c01944**.

31 A. Navarro-Huerta, T. Matsuo, A. S. Mikherdov, J. Blahut, E. Bartůňková, P. Jiang, M. Dračínský, S. Teat, M. Jin, S. Hayashi and B. Rodríguez-Molina, Optical Waveguiding Charge-Transfer Cocrystals: Examining the Impact of Molecular Rotations on Their Photoluminescence, *J. Am. Chem. Soc.*, 2025, **147**(10), 8343–8349, DOI: **10.1021/jacs.4c15957**.

32 P. Kautny, D. Lumpi, Y. Wang, A. Tissot, J. Bintinger, E. Horkel, B. Stöger, C. Hametner, H. Hagemann, D. Ma and J. Fröhlich, Oxadiazole Based Bipolar Host Materials Employing Planarized Triarylamine Donors for RGB PHOLEDs with Low Efficiency Roll-Off, *J. Mater. Chem. C*, 2014, **2**(11), 2069–2081, DOI: **10.1039/C3TC32338B**.

33 H. Puntscher, P. Kautny, B. Stöger, A. Tissot, C. Hametner, H. R. Hagemann, J. Fröhlich, T. Baumgartner and D. Lumpi, Structure–Property Studies of P-Triarylamine-Substituted Dithieno[3,2-*b*:2′,3′-*d*]Phospholes, *RSC Adv.*, 2015, **5**(114), 93797–93807, DOI: **10.1039/C5RA13651B**.

34 Y. Im, S. H. Han and J. Y. Lee, Dibenzothiophene and Indolocarbazole Cored Bipolar Hosts for Blue Phosphorescent Organic Light-Emitting Diodes, *Org. Electron.*, 2018, **62**, 560–565, DOI: **10.1016/j.orgel.2018.06.031**.

35 P. Kautny, Z. Wu, J. Eichelter, E. Horkel, B. Stöger, J. Chen, D. Ma, J. Fröhlich and D. Lumpi, Indolo[3,2,1-*jk*]carbazole Based Planarized CBP Derivatives as Host Materials for PhOLEDs with Low Efficiency Roll-Off, *Org. Electron.*, 2016, **34**, 237–245, DOI: **10.1016/j.orgel.2016.04.036**.

36 W. Cao, M. Fang, Z. Chai, H. Xu, T. Duan, Z. Li, X. Chen, J. Qin and H. Han, New D–π–A Organic Dyes Containing a *tert*-Butyl-Capped Indolo[3,2,1-*jk*]carbazole Donor with Bithiophene Unit as π-Linker for Dye-Sensitized Solar Cells, *RSC Adv.*, 2015, **5**(42), 32967–32975, DOI: **10.1039/C5RA02720A**.

37 C. Luo, W. Bi, S. Deng, J. Zhang, S. Chen, B. Li, Q. Liu, H. Peng and J. Chu, Indolo[3,2,1-*jk*]carbazole Derivatives-Sensitized Solar Cells: Effect of π-Bridges on the Performance of Cells, *J. Phys. Chem. C*, 2014, **118**(26), 14211–14217, DOI: **10.1021/jp503455m**.

38 Y. Hiraga, R. Kuwahara and T. Hatta, Novel Indolo[3,2,1-*jk*]carbazole-Based Bipolar Host Material for Highly Efficient Thermally Activated Delayed-Fluorescence Organic Light-Emitting Diodes, *Tetrahedron*, 2021, **94**, 132317, DOI: **10.1016/j.tet.2021.132317**.

39 Z.-P. Yan, M.-X. Mao, Q.-M. Liu, L. Yuan, X.-F. Luo, X.-J. Liao, W. Cai and Y.-X. Zheng, Rigidity-Enhanced Narrowband Iridium(III) Complexes with Finely-Optimized Emission Spectra for Efficient Pure-Red Electroluminescence, *Adv. Funct. Mater.*, 2024, **34**(38), 2402906, DOI: **10.1002/adfm.202402906**.

40 C. Zhao, T. Schwartz, B. Stöger, F. J. White, J. Chen, D. Ma, J. Fröhlich and P. Kautny, Controlling Excimer Formation in Indolo[3,2,1-*jk*]carbazole/9H-Carbazole Based Host Materials for RGB PhOLEDs, *J. Mater. Chem. C*, 2018, **6**(37), 9914–9924, DOI: **10.1039/C8TC03537G**.

41 T. Kader, B. Stöger, J. Fröhlich and P. Kautny, Azaindolo[3,2,1-*jk*]carbazoles: New Building Blocks for Functional Organic Materials, *Chem. – Eur. J.*, 2019, **25**(17), 4412–4425, DOI: **10.1002/chem.201805578**.

42 Y. Im, S. H. Han and J. Y. Lee, CN Substituted Indolocarbazole as a Core Structure of Exciton Harvesting and Lifetime

Extending Host for Green Thermally Activated Delayed Fluorescent Emitter, *Dyes Pigm.*, 2019, **164**, 233–236, DOI: 10.1016/j.dyepig.2019.01.024.

43 Y. Im, S. H. Han and J. Y. Lee, Deep Blue Thermally Activated Delayed Fluorescent Emitters Using CN-Modified Indolocarbazole as an Acceptor and Carbazole-Derived Donors, *J. Mater. Chem. C*, 2018, **6**(18), 5012–5017, DOI: 10.1039/C8TC00546J.

44 G. Szafraniec-Gorol, A. Slodek, D. Zych, M. Vasylieva, M. Siwy, K. Sulowska, S. Maćkowski, I. Taydakov, D. Goriachiy and E. Schab-Balcerzak, Impact of the Donor Structure in New D–π–A Systems Based on Indolo[3,2,1-*Jk*]Carbazoles on Their Thermal, Electrochemical, Optoelectronic and Luminescence Properties, *J. Mater. Chem. C*, 2021, **9**(23), 7351–7362, DOI: 10.1039/D1TC01208H.

45 V. V. Patil, K. H. Lee and J. Y. Lee, Universal Blue Emitters for High Efficiency Thermally Activated Delayed Fluorescence and Fluorescent Organic Light-Emitting Diodes, *Dyes Pigm.*, 2020, **174**, 108070, DOI: 10.1016/j.dyepig.2019.108070.

46 X.-J. Ma, X.-D. Zhu, K.-L. Wang, F. Igbari, Y. Yuan, Y. Zhang, C.-H. Gao, Z.-Q. Jiang, Z.-K. Wang and L.-S. Liao, Planar Starburst Hole-Transporting Materials for Highly Efficient Perovskite Solar Cells, *Nano Energy*, 2019, **63**, 103865, DOI: 10.1016/j.nanoen.2019.103865.

47 S. I. Wharton, J. B. Henry, H. McNab and A. R. Mount, The Production and Characterisation of Novel Conducting Redox-Active Oligomeric Thin Films From Electrooxidised Indolo[3,2,1-Jk]Carbazole, *Chem. – Eur. J.*, 2009, **15**(22), 5482–5490, DOI: 10.1002/chem.200900097.

48 W. Chen, L. Dang, Z. Situ, S. Ni, Y. Chen, S. Zhu, H. Li, S.-L. Chen, D. L. Phillips and M.-D. Li, Near-Infrared Light Triggered a High Temperature Utilizing Donor–Acceptor Cocrystals, *J. Phys. Chem. Lett.*, 2022, **13**(28), 6571–6579, DOI: 10.1021/acs.jpclett.2c01037.

49 P. Shi, X.-X. Liu, X.-L. Dai, T.-B. Lu and J.-M. Chen, Near-Infrared Photothermal Conversion Properties of Carbazole-Based Cocrystals with Different Degrees of Charge Transfer, *CrystEngComm*, 2022, **24**(25), 4622–4628, DOI: 10.1039/D2CE00523A.

50 D. Zhang, S. Li, S. Gao, S. Fu, K. Liu, D. He, H. Liu, X. Zhang and W. Hu, NIR-II Organic Photothermal Cocrystals with Strong Charge Transfer Interaction for Flexible Wearable Heaters, *Chin. J. Chem.*, 2024, **42**, 1563–1570, DOI: 10.1002/cjoc.202300738.

51 Y. Chen, J. Li and J. Gong, Jumping Crystal Based on an Organic Charge Transfer Complex with Reversible ON/OFF Switching of Luminescence by External Thermal Stimuli, *ACS Mater. Lett.*, 2021, **3**(3), 275–281, DOI: 10.1021/acsmaterialslett.0c00575.

52 N. R. Goud and A. J. Matzger, Impact of Hydrogen and Halogen Bonding Interactions on the Packing and Ionicity of Charge-Transfer Cocrystals, *Cryst. Growth Des.*, 2017, **17**(1), 328–336, DOI: 10.1021/acs.cgd.6b01548.

53 A. Mandal, A. Choudhury, R. Kumar, P. K. Iyer and P. Mal, Exploring the Semiconductor Properties of a Charge Transfer Cocrystal of 1-Aminopyrene and TCNQ, *CrystEngComm*, 2020, **22**(4), 720–727, DOI: 10.1039/C9CE01507H.

54 P. Makuła, M. Pacia and W. Macyk, How To Correctly Determine the Band Gap Energy of Modified Semiconductor Photocatalysts Based on UV-Vis Spectra, *J. Phys. Chem. Lett.*, 2018, **9**(23), 6814–6817, DOI: 10.1021/acs.jpclett.8b02892.

55 P. Hu, K. Du, F. Wei, H. Jiang and C. Kloc, Crystal Growth, HOMO–LUMO Engineering, and Charge Transfer Degree in Perylene-FxTCNQ (x = 1, 2, 4) Organic Charge Transfer Binary Compounds, *Cryst. Growth Des.*, 2016, **16**(5), 3019–3027, DOI: 10.1021/acs.cgd.5b01675.

56 D. Nanova, S. Beck, A. Fuchs, T. Glaser, C. Lennartz, W. Kowalsky, A. Pucci and M. Kroeger, Charge Transfer in Thin Films of Donor–Acceptor Complexes Studied by Infrared Spectroscopy, *Org. Electron.*, 2012, **13**(7), 1237–1244, DOI: 10.1016/j.orgel.2012.02.021.

57 B. Mahns, O. Kataeva, D. Islamov, S. Hampel, F. Steckel, C. Hess, M. Knupfer, B. Büchner, C. Himcinschi, T. Hahn, R. Renger and J. Kortus, Crystal Growth, Structure, and Transport Properties of the Charge-Transfer Salt Picene/2,3,5,6-Tetrafluoro-7,7,8,8-Tetracyanoquinodimethane, *Cryst. Growth Des.*, 2014, **14**(3), 1338–1346, DOI: 10.1021/cg401841n.

58 A. Salmerón-Valverde, J. G. Robles-Martínez, J. García-Serrano, R. Gómez, R. M. Ridaura, M. Quintana and A. Zehe, A Study of the Degree of Charge Transfer in TTF Molecular Complexes with Nitro-Carboxylated Fluorene Derivatives, *Mol. Eng.*, 1999, **8**(4), 419–426, DOI: 10.1023/A:1008384013189.

59 J. S. Chappell, A. N. Bloch, W. A. Bryden, M. Maxfield, T. O. Poehler and D. O. Cowan, Degree of Charge Transfer in Organic Conductors by Infrared Absorption Spectroscopy, *J. Am. Chem. Soc.*, 1981, **103**(9), 2442–2443, DOI: 10.1021/ja00399a066.

60 S. Matsuzaki, R. Kuwata and K. Toyoda, Raman Spectra of Conducting TCNQ Salts; Estimation of the Degree of Charge Transfer from Vibrational Frequencies, *Solid State Commun.*, 1980, **33**(4), 403–405, DOI: 10.1016/0038-1098(80)90429-9.

61 J. Gao, J. Guo, Y. Chen, S. Deng, Q. Lu, Y. Ren, X. Wang, H. Fan, F. Teng, X. He, H. Jiang and P. Hu, The Competitive Role of C–H···X (X = F, O) and π–π Interactions in Contributing to the Degree of Charge Transfer in Organic Cocrystals: A Case Study of Heteroatom-Free Donors with p-Fluoranil (FA), *CrystEngComm*, 2022, **24**(36), 6429–6438, DOI: 10.1039/D2CE00925K.

62 M. A. Spackman and D. Jayatilaka, Hirshfeld Surface Analysis, *CrystEngComm*, 2009, **11**(1), 19–32, DOI: 10.1039/B818330A.

63 J. P. Perdew, K. Burke and M. Ernzerhof, Generalized Gradient Approximation Made Simple, *Phys. Rev. Lett.*, 1996, **77**(18), 3865–3868, DOI: 10.1103/PhysRevLett.77.3865.

64 M. J. Frisch, G. W. Trucks, H. B. Schlegel, G. E. Scuseria, M. A. Robb, J. R. Cheeseman, G. Scalmani, V. Barone, B. Mennucci, G. A. Petersson, H. Nakatsuji, M. Caricato, X. Li, H. P. Hratchian, A. F. Izmaylov, J. Bloino, G. Zheng, J. L. Sonnenberg, M. Hada, M. Ehara, K. Toyota, R. Fukuda, J. Hasegawa, M. Ishida, T. Nakajima, Y. Honda, O. Kitao, H. Nakai, T. Vreven, J. A. Montgomery, Jr., J. E. Peralta,

F. Ogliaro, M. Bearpark, J. J. Heyd, E. Brothers, K. N. Kudin, V. N. Staroverov, R. Kobayashi, J. Normand, K. Raghavachari, A. Rendell, J. C. Burant, S. S. Iyengar, J. Tomasi, M. Cossi, N. Rega, J. M. Millam, M. Klene, J. E. Knox, J. B. Cross, V. Bakken, C. Adamo, J. Jaramillo, R. Gomperts, R. E. Stratmann, O. Yazyev, A. J. Austin, R. Cammi, C. Pomelli, J. W. Ochterski, R. L. Martin, K. Morokuma, V. G. Zakrzewski, G. A. Voth, P. Salvador, J. J. Dannenberg, S. Dapprich, A. D. Daniels, Ö. Farkas, J. B. Foresman, J. V. Ortiz, J. Cioslowski and D. J. Fox, *Gaussian 09 Revision E.01*, Gaussian, Inc., Wallingford, 2009.

65 T. Yanai, D. P. Tew and N. C. Handy, A New Hybrid Exchange–Correlation Functional Using the Coulomb-Attenuating Method (CAM-B3LYP), *Chem. Phys. Lett.*, 2004, **393**(1), 51–57, DOI: **10.1016/j.cplett.2004.06.011**.

66 S. Grimme, J. Antony, S. Ehrlich and H. Krieg, A Consistent and Accurate Ab Initio Parametrization of Density Functional Dispersion Correction (DFT-D) for the 94 Elements H-Pu, *J. Chem. Phys.*, 2010, **132**(15), 154104, DOI: **10.1063/1.3382344**.

67 K. P. Goetz, D. Vermeulen, M. E. Payne, C. Kloc, L. E. McNeil and O. D. Jurchescu, Charge-Transfer Complexes: New Perspectives on an Old Class of Compounds, *J. Mater. Chem. C*, 2014, **2**(17), 3065–3076, DOI: **10.1039/C3TC32062F**.

68 A. Colin-Molina, D. P. Karothu, M. J. Jellen, R. A. Toscano, M. A. Garcia-Garibay, P. Naumov and B. Rodríguez-Molina, Thermosalient Amphidynamic Molecular Machines: Motion at the Molecular and Macroscopic Scales, *Matter*, 2019, **1**(4), 1033–1046, DOI: **10.1016/j.matt.2019.06.018**.

69 E. A. Hernández-Morales, A. Colin-Molina, J. Arcudia, F. J. Hernández, M. Rodríguez, R. A. Toscano, R. Crespo-Otero, G. Merino and B. Rodríguez-Molina, Indolocarbazole as a Platform for Concatenated Crystalline Rotors, *Cryst. Growth Des.*, 2023, **23**(9), 6785–6794, DOI: **10.1021/acs.cgd.3c00650**.

70 A. Torres-Huerta, D. Galicia-Badillo, A. Aguilar-Granda, J. T. Bryant, F. J. Uribe-Romo and B. Rodríguez-Molina, Multiple Rotational Rates in a Guest-Loaded, Amphidynamic Zirconia Metal–Organic Framework, *Chem. Sci.*, 2020, **11**(42), 11579–11583, DOI: **10.1039/D0SC04432F**.

71 A. Acosta-Vera, D. Galicia-Badillo, A. Navarro-Huerta, K. Stracke, V. Gómez-Vidales, J. Rodríguez-Hernández, J. D. Evans and B. Rodríguez-Molina, Modulation of the Photophysics and Internal Dynamics in a Zr Metal Organic Framework by the Inclusion of Fluorinated Guests, *ACS Mater. Lett.*, 2024, **6**(9), 4395–4401, DOI: **10.1021/acsmaterialslett.4c00805**.

72 J. W. Christian, Characteristics of Martensitic Transformations, in *The Theory of Transformations in Metals and Alloys*, ed. J. W. Christian, Pergamon, Oxford, 2002, ch. 21, pp. 961–991, DOI: **10.1016/B978-008044019-4/50026-X**.

73 S. K. Park and Y. Diao, Martensitic Transition in Molecular Crystals for Dynamic Functional Materials, *Chem. Soc. Rev.*, 2020, **49**(22), 8287–8314, DOI: **10.1039/D0CS00638F**.

74 A. van der Lee and D. G. Dumitrescu, Thermal Expansion Properties of Organic Crystals: A CSD Study, *Chem. Sci.*, 2021, **12**(24), 8537–8547, DOI: **10.1039/D1SC01076J**.

75 B. K. Saha and R. V. P. Veluthaparambath, Roles of Molecular Volume, Surface Area, Heteroatoms, and Hydrogen Bonds on the Thermal Expansion of Organic Crystals, *Cryst. Growth Des.*, 2024, **24**(8), 3467–3472, DOI: **10.1021/acs.cgd.4c00199**.

76 M. J. Cliffe and A. L. Goodwin, PASCal: A Principal Axis Strain Calculator for Thermal Expansion and Compressibility Determination, *J. Appl. Crystallogr.*, 2012, **45**(6), 1321–1329, DOI: **10.1107/S0021889812043026**.

77 A. L. Goodwin, M. Calleja, M. J. Conterio, M. T. Dove, J. S. O. Evans, D. A. Keen, L. Peters and M. G. Tucker, Colossal Positive and Negative Thermal Expansion in the Framework Material $Ag_3[Co(CN)_6]$, *Science*, 2008, **319**(5864), 794–797, DOI: **10.1126/science.1151442**.

78 V. G. Saraswatula, D. Sharada and B. K. Saha, Stronger $\Pi\cdots\pi$ Interaction Leads to a Smaller Thermal Expansion in Some Charge Transfer Complexes, *Cryst. Growth Des.*, 2018, **18**(1), 52–56, DOI: **10.1021/acs.cgd.7b01502**.

79 R. L. Silvestri and J. L. Koenig, A T1 Spin-Lattice Relaxation and a Cross-Polarization Dynamics Study of the Molecular Motions of a Side-Chain Liquid Crystalline Polymer, *Macromolecules*, 1992, **25**(9), 2341–2350, DOI: **10.1021/ma00035a010**.